Available online at BCREC website: https://bcrec.id

Bulletin of Chemical Reaction Engineering & Catalysis, 18 (1) 2023, 25-36

Research Article

Nickel/Biochar from Palm Leaves Waste as Selective Catalyst for Producing Green Diesel by Hydrodeoxygenation of Vegetable Oil

Galih Dwiki Ramanda[1], A. Allwar[1], Muchammad Tamyiz[2,3], Is Fatimah[1], Ruey-an Doong[2]

[1]Department of Chemistry, Faculty of Mathematics and Natural Sciences, Universitas Islam Indonesia, Kampus Terpadu UII, Jl. Kaliurang Km 14, Sleman, Yogyakarta, 55584, Indonesia
[2]Universitas Nahdlatul Ulama Sidoarjo, Jl. Lingkar Timur KM 5, 5 Rangkah Kidul, Kecamatan Sidoarjo, Sidoarjo, 61234, Indonesia
[3]Institute of Analytical and Environmental Sciences, National Tsing Hua University, 101, Sec 2, Kuang Fu Road, Hsinchu, 30013, Taiwan.

Received: 9th November 2022; Revised: 7th January 2023; Accepted: 8th January 2023
Available online: 13rd January 2023; Published regularly: March 2023

Abstract

The objective of this research was to prepare low-cost catalyst for green diesel conversion from vegetable oil. The catalyst of nickel-dispersed biochar (Ni/BC) was prepared by direct pyrolysis of nickel precursor with palm leaves waste under N_2 stream at 500 °C. The obtained catalyst was examined by using x-ray diffraction, scanning electron microscope-energy dispersive x-ray, transmission electron microscopy, gas sorption analysis, FTIR and surface acidity examination. The catalytic activity testing was performed on rice bran oil hydrodeoxygenation at varied temperature and time of reaction. Based on analyses, the results showed the successful preparation of Ni/BC with the characteristic of single nickel nanoparticles decorated on surface. The increasing specific surface area of material was conclusively remarked the surface area enhancement by nickel dispersion along with the increased surface acidity, suggesting that the material can be applied for acid catalysis applications. The Ni/BC exhibited excellent catalytic conversion of rice bran oil with the high selectivity toward diesel fraction with 85.3% yield and 92.6% selectivity.

Keywords: Biochar; Catalyst; Hydrodeoxygenation; Green diesel

How to Cite: G.D. Ramanda, A. Allwar, M. Tamyiz, I. Fatimah, R. Doong (2023). Nickel/Biochar from Palm Leaves Waste as Selective Catalyst for Producing Green Diesel by Hydrodeoxygenation of Vegetable Oil. *Bulletin of Chemical Reaction Engineering & Catalysis*, 18(1), 25-36 (doi: 10.9767/bcrec.16403)

Permalink/DOI: https://doi.org/10.9767/bcrec.16403

1. Introduction

The increase in energy demand and the limited crude oil reserves are the main concerns in recent years. These forced continuous efforts to explore alternative and renewable fuel sources. Progressive investigations have shown the feasibility of biomass-based fuel produced by catalytic cracking processes. Due to the potency in cultivation, vegetable oils, such as sunflower oil, soybean oil, palm oil, *etc*., are compatible as production feedstock. Catalytic deoxygenation for upgrading vegetable oil feedstocks into green fuels, mainly green diesel is valued to be potential in the future.

In the sustainability perspective, the development of low-cost technology by designing low-cost catalytic process is also important. Catalysts based on nickel (Ni), molybdenum (Mo) and platinum (Pt) are widely used and well-known for hydrocracking mechanism. Beside of

* Corresponding Author.
Email: isfatimah@uii.ac.id (I. Fatimah);
Telp: +62-274-896 439 Fax: +62-274-895 920

their activity and selectivity in the cracking mechanism, the stability of active metals can be achieved by their dispersion onto solid supports, mainly porous supports [1,2]. Within this scheme, carbon-based catalysts especially biochar-based catalysts are recently proposed to be sustainable and low-cost materials for energy preservation.

Palm fruit is the strategic agricultural plant for some strategic industrial sectors in Indonesia and some Asian countries. Refer to sustainable development goal, many attempts are developed to enhanced the fruitful benefits from the palm industries by designing a circular economy route [3,4]. Beside of the use of palm oil waste and sludge, the utilization of solid waste is required to be intensified. Palm leaves is one of the huge plant wastes in palm oil industry which usually used only for the animal feed or natural fuel. Chemically, the lignocellulosic content in the leaves is potential to be developed for functional materials, one of these is to be biochar. Many advantageous can be utilized from the characteristics of the biochar such as adsorbent in wastewater treatment, and also being solid support material for many active catalytic compounds [3]. Previous research reported the economic competitiveness of the green fuel production from vegetable oils [5,6]. Biochar modified with metals; especially transitional metals is widely developed in catalysis area. For supporting catalytic in palm oil-based industries for example, nickel-supported biochar can be utilized as hydrogenation-based processes. Based on these backgrounds, in this research, preparation of nickel supported biochar from palm leaves was firstly reported.

The study was aimed to characterize the physicochemical character of the nickel-supported biochar as the basic information for further applications as catalyst in vegetable oil hydrocracking. Such instrumentations including x-ray diffraction (XRD), Fourier-Transform Infra-Red (FTIR), surface profile using scanning electron microscopy along with elemental analysis (SEM-EDX), and gas sorption analysis were employed. For catalytic activity test, the hydrocracking of rice bran oil (RBO) in a batch reaction system was applied.

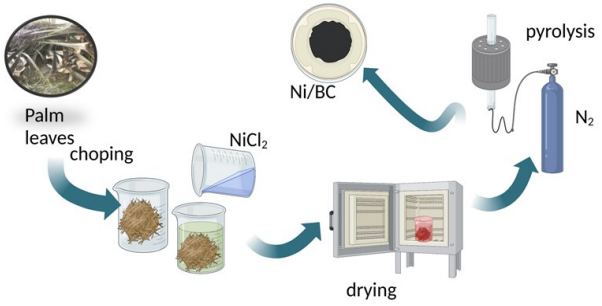

Figure 1. Schematic representation of Ni/BC preparation.

2. Materials and Methods

2.1 Materials

Palm leaves was obtained from West Kalimantan palm agricultural area. The leaves were cleaned and chop to get smaller size. Chemicals consist of nickel (II) chloride, NaOH, HCl, acetic acid, pyridine and n-butylamine were purchased from Merck (Darmstadt, Germany). Nitrogen gas (N_2) in ultra-high purity specification was supplied by PT. Samator Indonesia.

2.2 Preparation of Ni/BC

Ni/BC was prepared by mixing the chopped palm leaves with $NiCl_2$ solution until the Ni concentration set at 10 wt% in the composite. The mixture was dried in the oven before was pyrolyzed at the temperature of 500 °C for 1 h under N_2 gas flow. For comparison purposes, the unmodified-biochar (BC) was prepared with similar method but without any nickel mixing prior the pyrolysis step. Figure 1 presents the scheme of Ni/BC preparation.

2.3 Physicochemical Characterization

The physicochemical properties of the samples were characterized using field emission-scanning electron microscope (FE-SEM), transmission electron microscopy (TEM), x-ray diffraction (XRD), gas sorption analysis, and Fourier Transform Infra-Red (FTIR). A Phenom X instrument (US) was employed for SEM analysis, while TEM images were taken from JEOL TEM 2010 transition electron microscope operated at the applied voltage of 200 kV. XRD of XPERT-PRO with a Ni-filtered-Cu Kα radiation (λ = 0.154060 nm) was utilized for analysis with the range of 2-75°. A Thermonicolet Avatar Spectrophotometer (Madison, USA) was employed to examine FTIR spectra for identifying the changes of surface functional groups of the materials. Differential thermal analysis-gas sorption analysis (DTA-TGA) was performed on Seiko DTA/TGA-300.

2.4 Analysis of Acid Analysis and Surface Acidity

Acid group analysis was carried out by immersing 0.1 gram of biochar into 25 mL of each solution of 0.05 N $NaHCO_3$, 0.05 N Na_2CO_3 and

NaOH 0.05 N. The mixture was allowed to stand for 24 hours and filtered. A total of 5 mL of each filtrate was pipetted and put into an Erlenmeyer then added an excess of 0.05 N HCl solution (10 mL) and 2-3 drops of indicator. The analyte was back-titrated using 0.05 N NaOH [7].

Surface acidity of the samples was determined by using quantitative and qualitative method. The total surface acidity was determined by using back titration method using n-butylamine as base probe. The samples were mixed with excess amount of n-butylamine solution followed by stirring for 6 h for complete adsorption, and the rest of unadsorbed n-butylamine was determined by using acetic acid solution as standard solution. The total acidity was measured as mmol equivalent of acid to mass of the sample (mmol/g). Qualitatively, the ratio of Lewis to Brønsted acid (L/B) of the samples was calculated by the pyridine adsorption method. For the analysis, dried samples were evacuated in by vacuum pumped prior the pyridine vapor exposed in a desiccator. The pyridine adsorption was performed overnight, followed by analysis using Fourier-Transform Infra-Red (FTIR) analysis. The L/B value was calculated by using Equation (1) [8]:

$$\frac{L}{B} = \frac{Intensity\ of\ peak\ at\ wavenumber\ of\ 1450\ cm^{-1}}{Intensity\ of\ peak\ at\ wavenumber\ of\ 1540\ cm^{-1}} \quad (1)$$

2.5 Catalytic Activity Test

The prepared Ni/BC sample was examined as catalyst in RBO hydrocracking in a batch reactor. Particularly, for each testing the mixture of 0.2 g of catalyst and 25 g of RBO was set-up at a hydrogen pressure of 0.5 kPa. The reactor was then heated at set-up temperature for certain time of reaction. For all the experimental runs, the liquid from the reaction result was collected for furthermore analyzed with gas chromatography-mass spectrometry (GCMS). To characterize the product samples, 10 µL of the sample was filtered and then transferred into a GC-MS sample holder. The analysis was performed using Shimadzu on HP5 column (30 m × 0.25 µm ID × 250 µm) with argon used as the carrier gas. The activity of catalyst (%) and selectivity (%) of the reaction to produce gasoline (C_5-C_{10}), kerosene (C_{11}-C_{16}) and diesel fraction (C_{17}-C_{24}) were determined by using Equations (2) and (3).

$$Yield\ (\%) = \frac{A_{C_5-C_{24}}}{A_{total}} \times \frac{m_L}{m_F} \times 100\% \quad (2)$$

$$Selectivity\ (\%) = \frac{A_i}{A_{C_5-C_{24}}} \times 100\% \quad (3)$$

where, $A_{C5\text{-}C24}$ is the peak area of products with total carbon of 5 until 24, A_{total} is total peak area from GC measurement, m_L is mass of liquid product, m_F is mass of feed (RBO), and A_i is peak area of intended product (gasoline (C_5-C_{10}), kerosene (C_{11}-C_{16}), or diesel fraction (C_{17}-C_{24})).

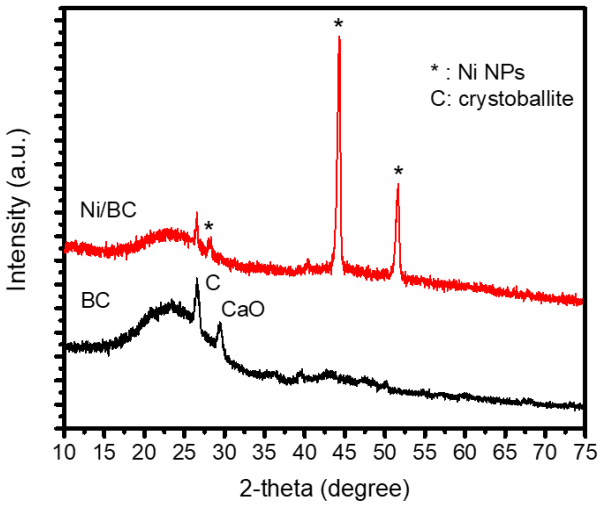

Figure 2. XRD patterns of BC and Ni/BC.

3. Results and Discussion

3.1 Physicochemical Characterization of Ni/BC

Powder XRD patterns for the BC and Ni/BC are recorded in Figure 2. The specific pattern of biochar is broad peak at 2θ ranging at 20°–30° refer to the small dimensions of crystallites perpendicular to aromatic layers and the structure of aromatic layers (graphite 002). In addition, sharp peaks are found at 2θ of 26° and 27° implying the miscellaneous inorganic components of cristobalite and calcite, respectively. Both minerals are related with that both compounds are the main constituent of agricultural media [9,10].

The XRD pattern of Ni/BC demonstrates the dispersed the nickel nanoparticles as indicated by the peaks at 2θ of 45°, 52.3°, and 77.4° refer to JCPDS: 03-1051 [11]. The reflections are associated with nickel with a structure of a-FCC with planes of 111, 200, and 222 suggest the single nickel nanoparticles dispersed onto biochar surface [11–13].

The change of the structure is reflected by the SEM images presented in Figure 3. BC sample shows a characteristic of the biochar consisting some hole of the surface representing the provided pores created by heating the lignocellulosic structure in biomass [14–17]. After modified with Ni, some lighter spots are

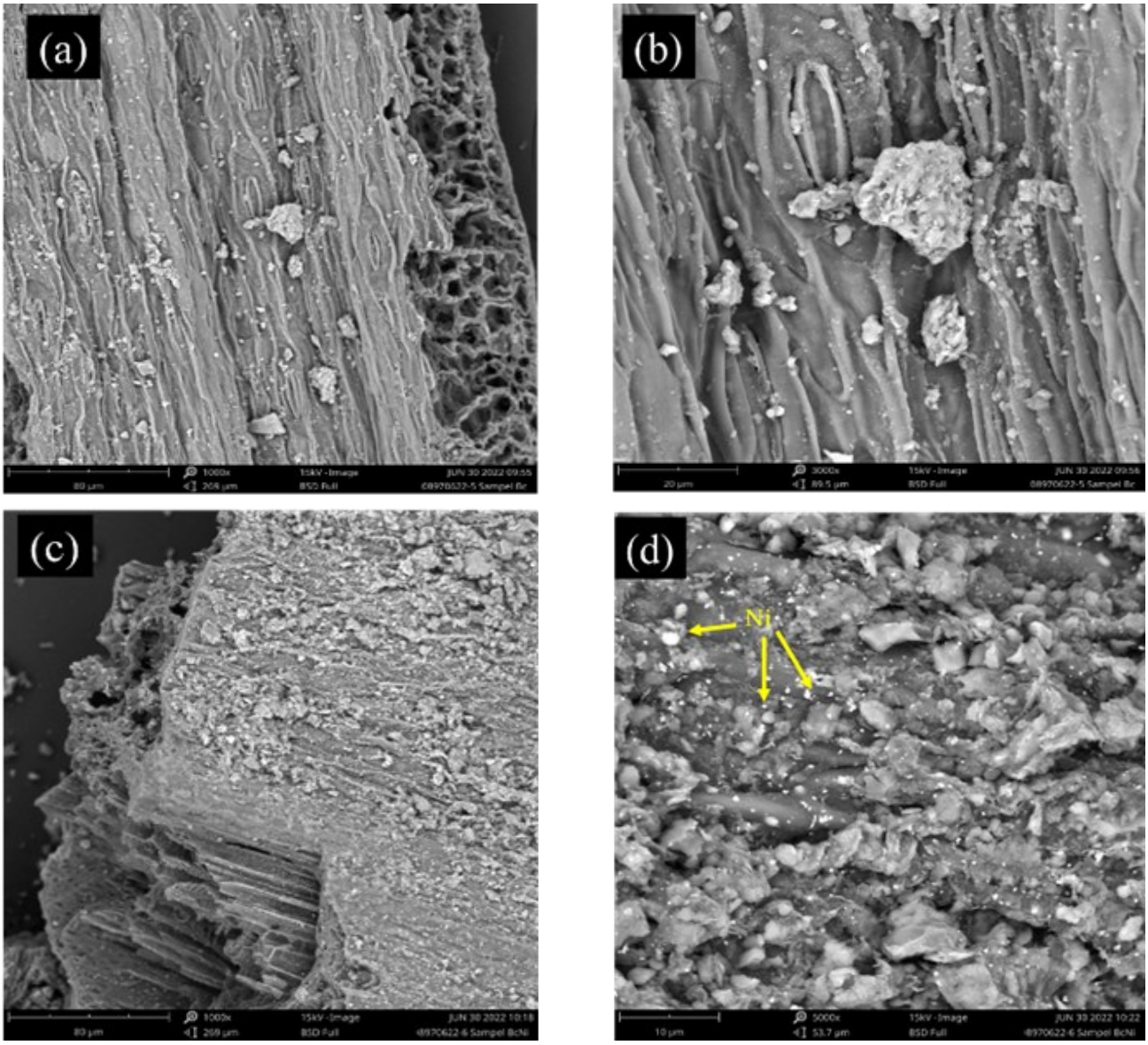

Figure 3. Surface images of (a-b) BC with different magnification (c-d) Ni/BC with different magnifications.

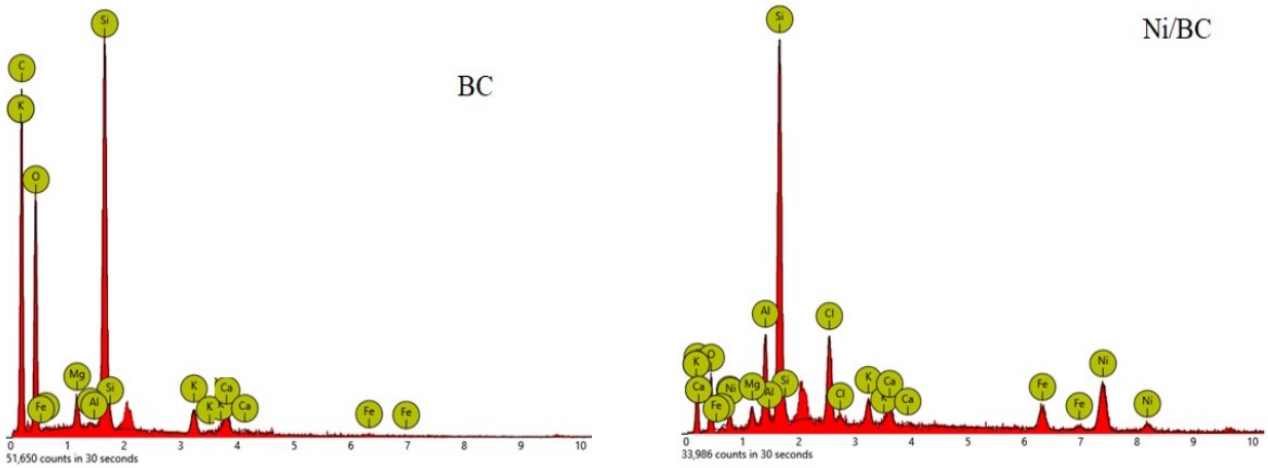

Figure 4. EDX spectra of BC and Ni/BC.

found on surface implying the dispersed Ni nanoparticles (Ni NPs). This is also reflected by EDX results in Figure 4. with elemental composition presented in Table 1. It is noted that the morphology of the dispersed Ni is different with similar material in previous work [18] which showed nanorods morphology. The different Ni concentration may affect to the crystallite growth of Ni NPs on the surface. By using Scherer equation presented elsewhere, the calculated nickel crystallite size from those peaks is 46 nm [19].

To ensure the dispersed nickel in the Ni/BC, TEM analysis was performed. TEM and HRTEM images and SAED pattern are presented in Figure 5. As can be seen from Figure 5(a) and 5(b), the dispersed spherical spots with the particle size ranging at 20-30 nm are identified in Ni/BC as the indication of the dispersed Ni nanoparticles, meanwhile the spots are not existed in the BC surface. By HRTEM analysis, the appeared fringes with the constant distance of 0.21 nm which associated with (111) space. In addition, the nanocrystal structure of Ni is reflected by two rings in the

Table 1. Elemental analysis of BC and Ni/BC from EDX analysis.

Element	Percentage in (wt%)	
	BC	Ni/BC
O	40.81	29.19
Ca	0.33	0.11
C	18.17	31.21
Al	12.42	7.57
Si	12.07	12.27
K	8.73	2.46
Fe	6.78	4.60
Mg	0.68	0.93
Ni	n.d	9.23

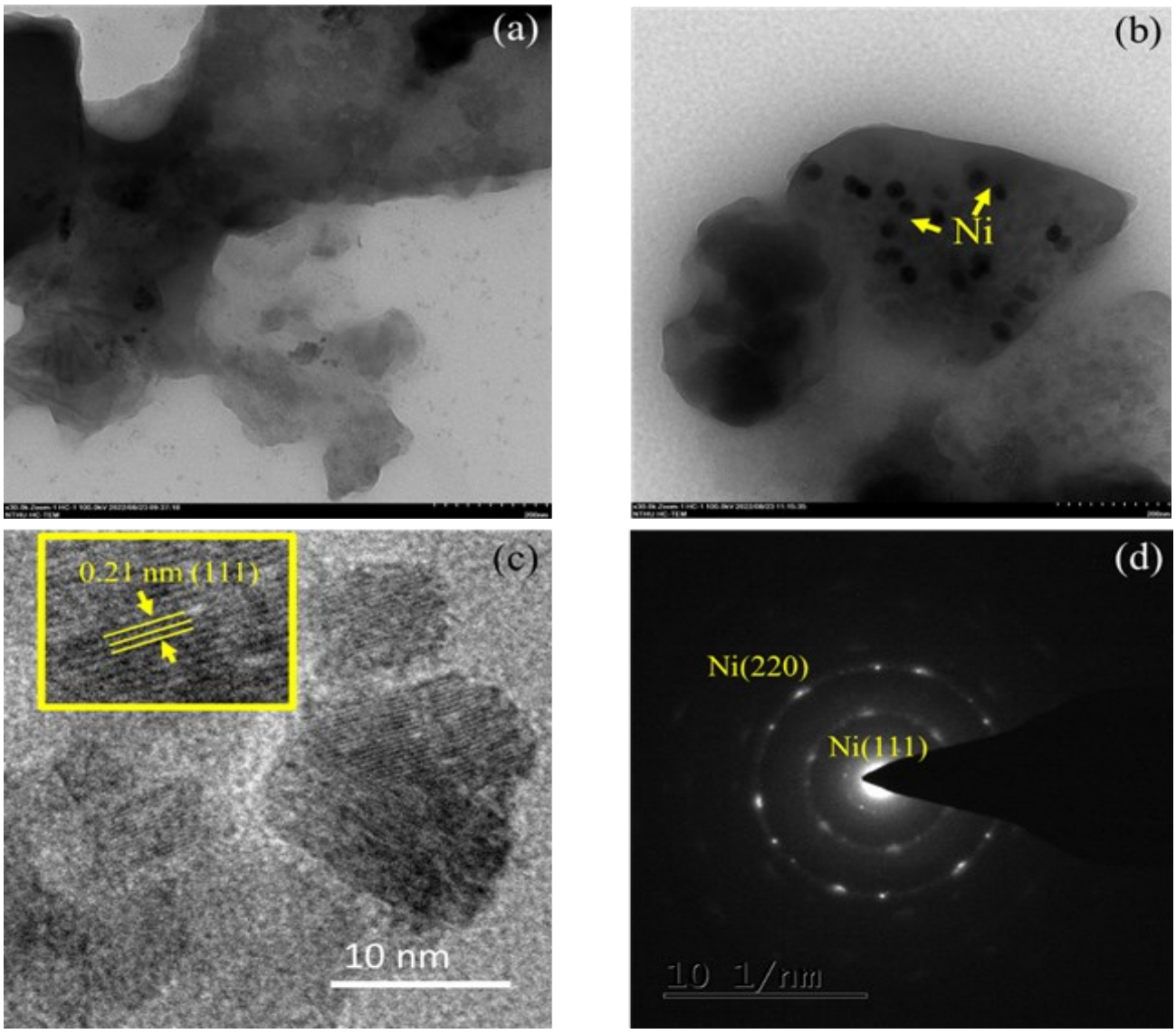

Figure 5. (a) TEM image of BC; (b-d) TEM, HRTEM images and SAED pattern of Ni/BC, respectively.

SAED pattern as a result of the close values of d-spacing associated with the lattice spacings of (111) and (220) (Figure 5(d)).

In addition, the effect of Ni attachment into the BC structure is also confirmed by some shifting of the functional groups which are associated with the change of binding energy of each atom presented by the FTIR analysis. The spectra are presented in Figure 6. From Figure 6, it is seen that the spectrum of Ni/BC is not significantly different with the spectrum BC. There are some peaks associated with the characteristics of biochar such as the peak at around 3420-3436 cm^{-1} together with peaks at 1036-1044 cm^{-1} indicating the presence of water contained in the materials. The peak at around 1560-1585 cm^{-1} which is the indication of C=O functional groups and the peaks at finger print (400-500 cm^{-1}) as the indication of the attached Ni into BC support [20–22]. The anchored Ni onto biochar structure is appeared from the shift of 3421 and 457 cm^{-1} peaks into the higher wavenumber as representation of the Ni-bonding causing higher vibration energy which is also reflected by the higher wavenumber of C=O peak.

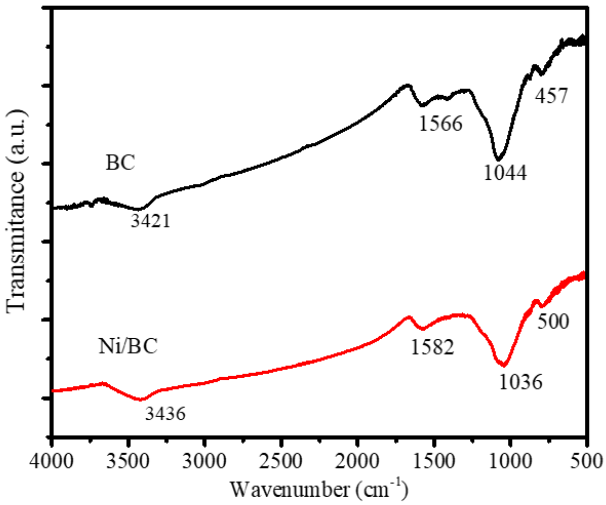

Figure 6. FTIR spectra of BC and Ni/BC.

Effect of nickel loading on biochar in Ni/BC on the surface profile was measured by using gas sorption analysis. Adsorption-desorption isotherm plots of Ni/BC in comparison with BC are depicted in Figure 7, and the calculated parameters based on the isotherm data are listed in Table 2. From isotherm plots (Figure 7(a)) of both BC and Ni/BC samples fit with type I of the IUPAC adsorption-desorption isotherm classification as the isotherms are parallel and horizontal parallel over the relative pressure range. The isotherm suggests that these materials have small mesopores and many micropores in their structure. This is also implied by the pore distribution determined from nitrogen desorption isotherms by the Barret-Joyner-

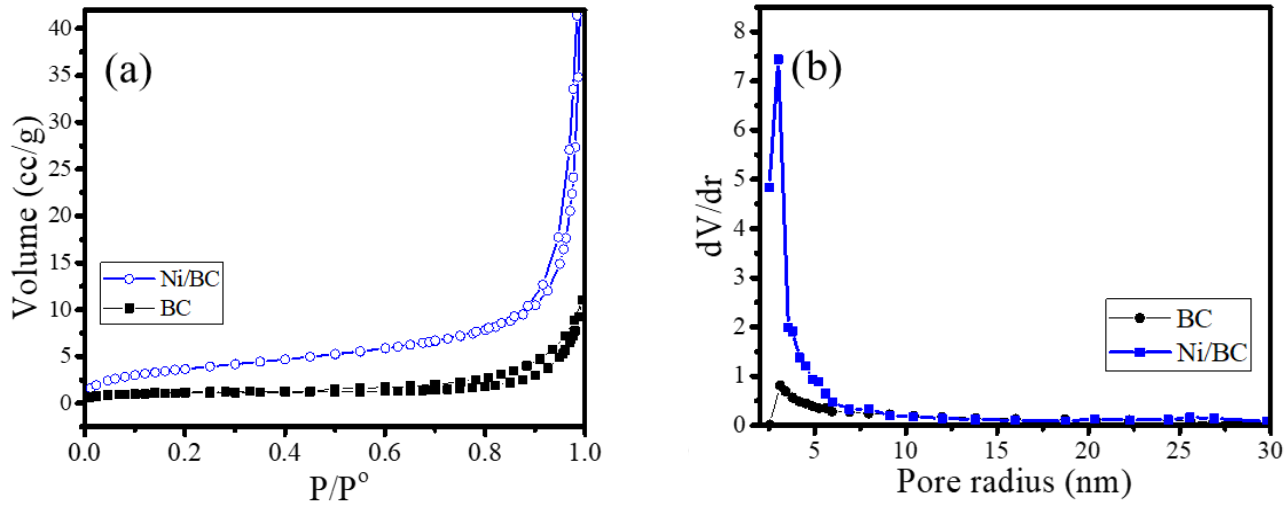

Figure 7. (a) Adsorption-desorption profile and (b) pore size distribution of BC and Ni/BC.

Table 2. Surface parameters obtained from gas sorption analysis of BC and Ni/BC.

Parameter	BC	Ni/BC
Specific surface area (m^2/g)	3.92	26.8
Pore volume (cm^3/g)	1.64×10^{-3}	3.75×10^{-3}
Pore diameter (nm)	16.36	18.08
Total acid group (meq/g)	24.6	24.85
Total surface acidity (mmol/g)	2.27	2.31
L/B	1.01	1.09

Halenda (BJH) presented in Figure 7(b) expressed the dominant pore diameter of around 2-5 nm in both materials, and calculated pore diameters for BC and Ni/BC are 16.36 and 18.08 nm, respectively. In more detail, the Ni/BC sample shows higher adsorption capability as the adsorbed volume is higher at all P/Po and pore radius ranges. The higher values of specific surface area and pore volume parameters are consequently obtained (Table 2).

An increasing specific surface area of material was found by Ni dispersion from 3.92 m^2/g to 26.80 m^2/g. It is in line with the surface morphology change suggesting the larger surface can adsorb nitrogen gas in the analysis method [23,24]. The higher volume capacity at the anchored nickel in the pores is related with the swelling capability of lignocellulosic decomposition during gasification/pyrolysis with the presence of nickel. In addition, impregnated nickel does not block the porosity, and this is similar with the trend reported by previous works [25,26].

The adsorption properties of the biochar are very influenced by the presence of an oxide group on the carbon surface. Oxide group on the surface of biochar can acidic can be determined by titration. Acidity of the carbon surface can be detected by the neutralization process using $NaHCO_3$ solution. Na_2CO_3, and NaOH. It is based on assumption that $NaHCO_3$ only neutralizes the carboxyl group on the carbon surface, Na_2CO_3 neutralizes the carboxyl group, lactones, and phenol groups. Characterized by using the Boehm titration method (*back titration*) and supported by analysis using FTIR. Total acid groups on surface modification of biochar before and after the modification is determined through the Boehm titration method as shown in Table 2.

The results show that the of activated carbon BC contains 24.60 $meq.g^{-1}$ total acid group. However, after the biochar was modified using metal Ni (Ni/BC), the results showed an increase in the total acid group by 24.85 $meq.g^{-1}$. This shows that by modifying the addition of Ni metal to biochar has extended the number of oxygen functional groups such as O−H, C=O, and C−OH. These results were relevance with the FTIR spectra of activated carbon under nitric acid (Figure 5) with appearing new peaks at bands 1560-1585 cm^{-1} which is an indication of the C=O functional group and the peaks on the fingerprint (400-500 cm^{-1}) as an indication of the presence of Ni metal on the surface of biochar.

Effect of immobilization of nickel in Ni/BC to the surface acidity is represented by the surface acidity measurement quantitative and qualitatively. The total acidity values counted as mmol of n-butylamine per mass of the catalyst (mmol/g) and the L/B ratio are also presented in Table 2. The L/B ratio is measured based on the FTIR spectra presented in Figure 8. Both samples show the absorption band at around 1450 cm^{-1} and 1540 cm^{-1} which are corresponding to the Lewis and Brønsted interaction of pyridine with available acid species, respectively [27,28]. It is seen that both total surface acidity and L/B of Ni/BC are higher compared to BC. The data represented that the presence of Ni on surface affect to the capability of surface to adsorb pyridine in Lewis interaction due to the possibility of electron pair or Lewis base site to bind with the *d*-orbital of Ni.

In order to make sure the stability of the Ni/BC for hydrodeoxygenation reaction until 500 °C, DTA-TGA analysis was performed, and thermogram is presented in Figure 9. According to TGA performance, fast weight loss up to

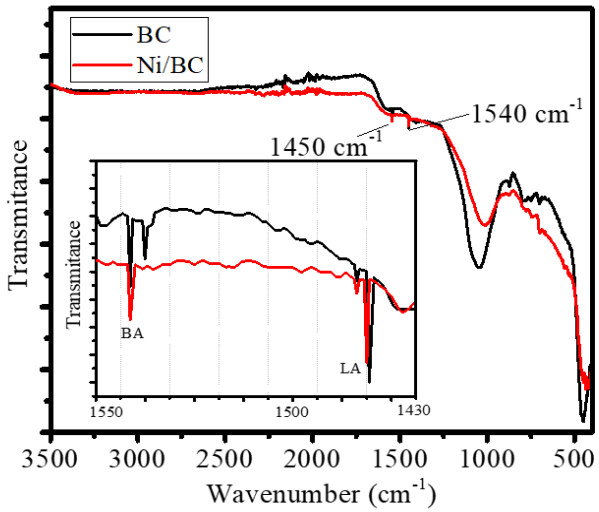

Figure 8. FTIR spectra of pyridine-adsorbed samples (LA: Lewis acid, BA: Brønsted acid).

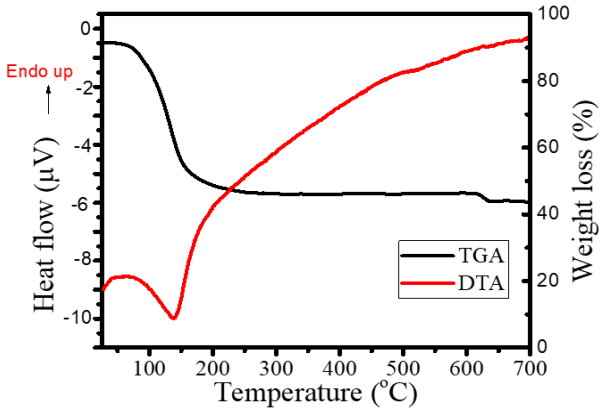

Figure 9. TGA-DTA of Ni/BC.

115 °C is identified due to the removal of surface adsorbed water. Afterwards, the increasing temperature is not significantly influencing the mass of the sample. The TGA pattern is in line with the DTA pattern that demonstrates the exothermic change refer to the loss of water weight, and consumed energy increased at the elevated temperature. Overall from both TGA and DTA profile, a stable Ni/BC at the range of 200-500 °C is mainly concluded, meaning that there is no subsequent decomposition of carbon.

3.2 Catalytic Activity of Ni/BC

The catalytic activity of Ni/BC was evaluated in the RBO hydrodeoxygenation under varied temperature and time of reaction. Initial evaluation of the chemical composition of RBO was performed by GC-MS analysis to the methylated RBO with the chromatogram depicted in Figure 10, and the composition is listed in Table 3. From the analysis, it is seen that oleic acid (69.83%) and palmitic acid (25.62%) are the major components of RBO, and other compounds of oleic acid, stearic acid, and lignoceric acid are presented as the minor component. Figure 11 presents the effect of temperature on the yield (%) and selectivity to kerosene fraction (C_{11}-C_{16}), and diesel fraction (C_{17}-C_{24}), from the reaction performed for 1 h.

At initial stage, the catalytic activity test to BC was conducted, and the reaction results were dominated by coke with small amount of hydrodeoxygenation result (<10%). Conclusively, the presence of nickel in Ni/BC is the major cause of the increasing yield. Refer to theoretical approach of heterogeneous catalysis mechanism, the specific surface area and surface acidity facilitated by nickel dispersion. These assumption is strengthened by study on the effect of temperature to the yield of reaction.

From Figure 11(a), it is seen that increasing temperature accelerated the catalytic performance as the higher yield obtained. This trend is in same trend with other vegetable oil deoxygenation over Ni-based catalyst which associated with the activated surface reaction between oil and catalyst surface [18,29]. In more detail, the compositional analysis to the products describes the different selectivity as produced by the different temperature (Figure 11(b)). The liquid product obtained at the reaction temperature of 200 °C and 300 °C are diesel fraction (C_{17}-C_{24}), meanwhile by the increasing temperature into 400 °C, the kerosene fraction products found. Mass spectrometric (MS) analysis to the liquid products obtained at 200 °C revealed that it is 16.5% of the liquid product is mainly diesel fraction and the rest heavy fraction of hydrocarbon (C>24). At higher temperature (400 and 500 °C), other smaller carbon products in kerosene fraction were produced which the selectivity of kerosene from 500 °C is higher than that of 400 °C. From MS analysis,

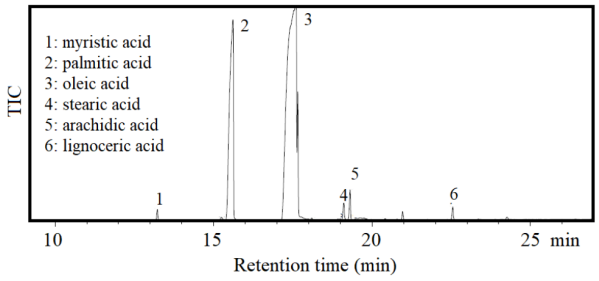

Figure 10. GC analysis results of RBO sample.

Table 3. Composition of RBO.

Peak No.	Compound	Percentage (%)
1	Myristic acid	0.40
2	Palmitic acid	25.62
3	Oleic acid	69.83
4	Stearic acid	0.82
5	Arachidic acid	1.20
6	Lignoceric acid	0.53

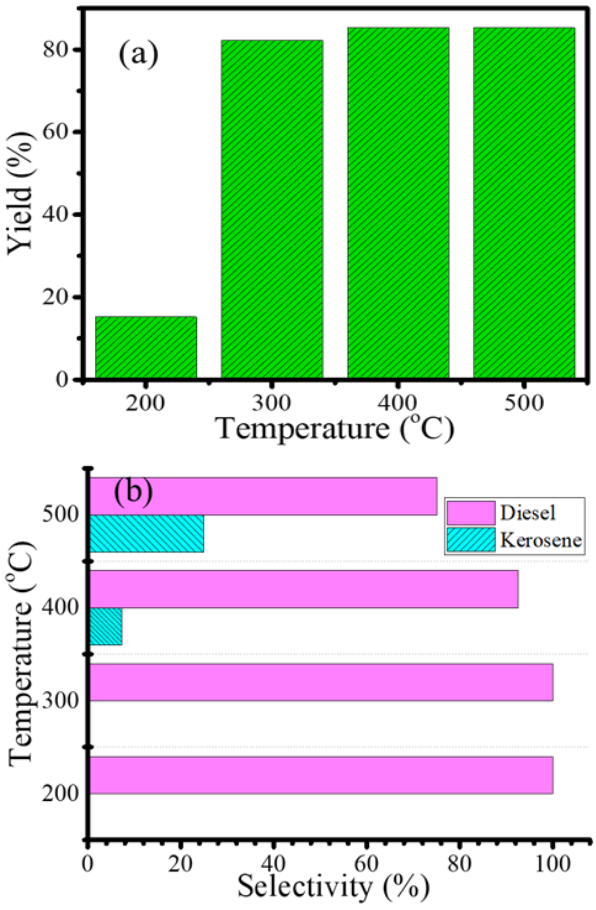

Figure 11. Effect of reaction temperature on (a) yield and (b) selectivity.

it found that the reaction product is a mixture of n-alkanes, and those from n-C_{15} up to n-C_{18} (mainly n-C_{17}) as the major components of the liquid product mixture. Detail analysis to the liquid product revealed that the compounds of dodecene, hexadecane, heptadec-8-ene, 1-Octadecene were detected. Figure 12 and Table 4 show the GC-MS analysis of the selected result. The presence of these compounds implies that hydrogenation, and generally deoxygenation mechanism including hydrodecarboxylation occurred at the temperature of 200 °C and 300 °C, and in addition, the hydrocracking is identified at the higher temperature.

The mechanism is supported by the results from the study of the effect of time of reaction to the yield and selectivity that are presented in Figure 13. The yield obtained from the reaction at 200 °C shows that the increasing time clearly contributed to the increasing yield, meaning that the higher volume of liquid product obtained. In more detail, diesel fraction is dominant component of the product of 1 and 2h, meanwhile by continuing the reaction until 3h, the kerosene fraction is obtained. Moreover, the smaller hydrocarbons in kerosene fraction of the yield from 3h reaction are the indication of hydrocracking mechanism as the continuing mechanism in a batch reaction system. Based on MS analyses to the compounds and considering that oleic acid is the dominant component of RBO, the general mechanism of hydrodeoxygenation can be described in some previous works [29].

Conclusively, the Ni/BC catalyst showed the selectivity to produce diesel fraction or usually called as green diesel regarding to the domination of hydrogenation and hydrodecarboxylation mechanism. At the higher temperature, even though there is reduced selectivity, but the tendency to produce green diesel is still dominant with increasing yield of reaction.

The possible mechanism and yield hydrodeoxygenation demonstrated in this work are similar with was reported in palm oil hydrodeoxygenation by Ni-MoS_2/γ-Al_2O_3 [31] and γ-Al_2O_3 supported Ni–Mo Catalysts [32]. Table

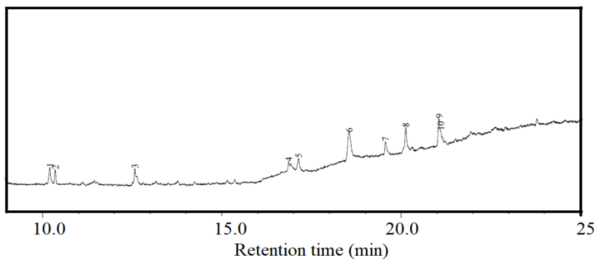

Figure 12. Chromatogram of hydrocracking result on Ni/BC catalyst [Time: 2 h, T: 500 °C)

Table 4. Composition of result (T: 500 °C, time: 2 h).

Peak No.	Compound	Percentage (%)
1	Olealdehyde	10.44
2	n-Pentadecane	7.14
3	9-Octadecene	4.99
4	Allyl stearate	6.65
5	Methyl oleate	5.83
6	1-Nonadecene	27.35
7	1-Octadecanol	6.47
8	9-Octadecenal	10.99
9	9-Octadecen-1-ol	16.27
10	Tetracosenoic acid methyl ester	3.85

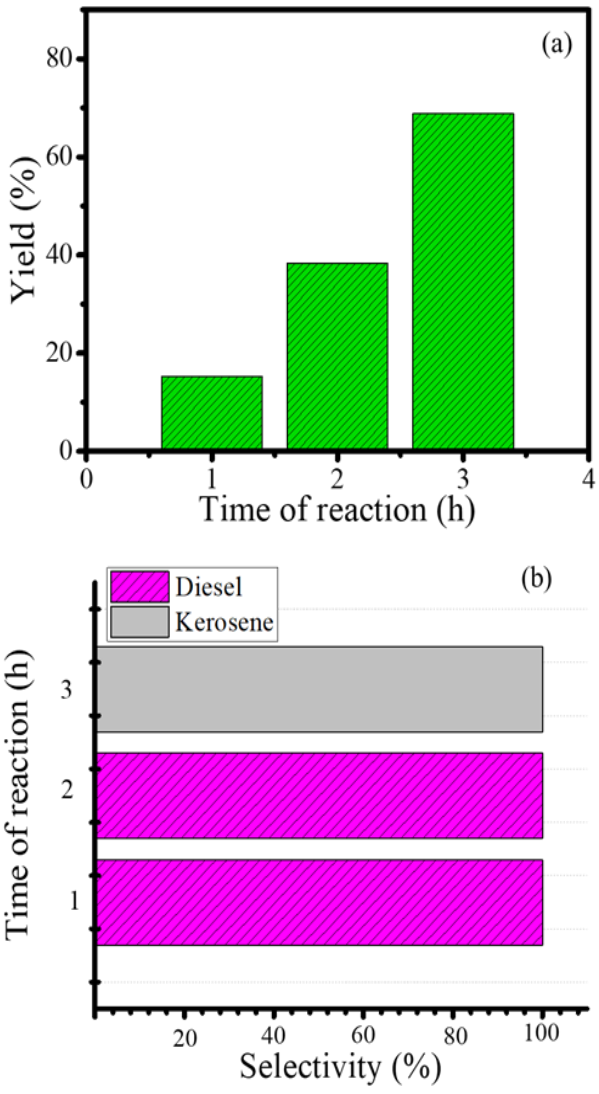

Figure 13. Effect of time of reaction on (a) yield and (b) selectivity.

5 lists comparison on catalytic activity of prepared catalyst in this work with other Ni-based catalyst for vegetable oil hydrodeoxygenation. From the comparison it is implied that that the prepared catalyst in this work has remarkable selectivity for producing green diesel.

4. Conclusion

Nickel-decorated biochar from palm leaves has been successfully synthesized with one-pot synthesis method. From XRD and TEM analyses, it was obtained that single phase of Ni NPs was identified on surface, meanwhile from SEM-EDX and gas sorption analysis, the enhanced surface area was created. The obtained material showed the enhanced performance related with specific surface area and surface acidity that facilitate the catalytic activity in rice bran oil hydrodeoxygenation.

Acknowledgement

Research support from Laboratory of Materials for Energy and Environment, Chemistry Department, Universitas Islam Indonesia was acknowledged.

CRediT Author Statement

Galih Dwiki Ramanda: Data curation, Formal analysis, Writing draft; Allwar: Conceptualization; Formal analysis; Muchammad Tamyiz: Formal analysis, Is Fatimah: Methodology, Roles/Writing - original draft; Writing - review & editing; Ruey-an Soong: Resources, Software, Supervision.

References

[1] Mampuru, M.B., Nkazi, D.B., Mukaya, H.E. (2020). Hydrocracking of waste cooking oil into biogasoline in the presence of a bifunctional Ni-Mo/alumina catalyst. *Energy Sources, Part A: Recovery, Utilization, and Environmental Effects*, 42 (20), 2564–2575. DOI: 10.1080/15567036.2019.1610527.

[2] Alisha, G.D., Trisunaryanti, W., Syoufian, A. (2022). Hydrocracking of Waste Palm Cooking Oil into Hydrocarbon Compounds over Mo Catalyst Impregnated on SBA-15. *Silicon*, 14 (5), 2309–2315. DOI: 10.1007/s12633-021-01035-1.

[3] Wardhani, R., Rahadian, Y. (2021). Sustainability strategy of Indonesian and Malaysian palm oil industry: a qualitative analysis. *Sustainability Accounting, Management and Policy Journal*, 12 (5), 1077–1107. DOI: 10.1108/SAMPJ-07-2020-0259.

[4] Raharja, S., Djohar, S., Aryanthi, D. (2021). Development Strategy of Indonesian Palm Oil Industrial Cluster Based International Trade Connectivity. *International Journal of Oil Palm*, 4 (2), 31–38. DOI: 10.35876/ijop.v4i2.59.

[5] Warid, F., Zainol, I., Abbass, N.M., Rahim, N., Majhool, A.A. (2020). Catalysis deoxygenation and hydrodeoxygenation of edible and inedible oil to green fuel. *Journal of Advanced Research in Fluid Mechanics and Thermal Sciences*, 74 (2), 146–159. DOI: 10.37934/ARFMTS.74.2.146159.

[6] Tran, C.C., Akmach, D., Kaliaguine, S. (2020). Hydrodeoxygenation of vegetable oils over biochar supported bimetallic carbides for producing renewable diesel under mild conditions. *Green Chemistry*, 22 (19), 6424–6436. DOI: 10.1039/d0gc00680g.

Table 5. Comparison on Ni/BC activity with other Ni-based catalyst for vegetable oil's deoxygenation.

Catalyst	Yield (%)	Selectivity to green diesel (%)	Remark	Reference
Ni/SiO_2-Al_2O_3	70	28	The reaction was utilizing rapeseed oil as feed, T = 300 °C, p = 70 bar, duration = 4 h	[18]
Ni/MWCNT	80	64	The highest yield and selectivity was achieved from the 1st -cycle reaction at 350 °C, 1 h, 10 mbar, 400 rpm. The feed is Jatropha curcas oil	[33]
Ni/Mordenite	100	56	Reaction was in flow-reactor of 350 °C.	[34]
Ni-Mo/γ-Al_2O_3	97	-	The feed was methyl ester, reaction conducted at 300 °C	[35]
Ni/SBA-15	85.1	78	Feed was palm oil, reaction in batch reactor at 350 °C under N_2 flow for 3 h.	[30]
Ni/BC	85.2	92.6	Feed of reaction is RBO, reaction at batch reactor 400 °C for 1 h under H_2 stream (0.2 kPa)	This work

[7] Akl, M.A., Youssef, A.F.M. (2016). Synthesis, Characterization and Evaluation of Peanut Shells-Derived Activated Carbons for Removal of Methomyl from Aqueous Solutions. *Journal of Environmental and Analytical Toxicology*, 6(2), 352. DOI: 10.4172/2161-0525.1000352.

[8] Fatimah, I., Rubiyanto, D., Huda, T., Handayani, S., Ilahi, O.M. (2015). Ni Dispersed on Sulfated Zirconia Pillared Montmorillonite as Bifunctional Catalyst in Eco-Friendly Citronellal Conversion. *Engineering Journal*, 19(5), 43–53. DOI: 10.4186/ej.2015.19.5.43.

[9] Arkaan, M.F., Ekaputri, R.F., Fatimah, I., Kamari, A. (2020). Physicochemical and photocatalytic activity of hematite/biochar nanocomposite prepared from Salacca skin waste. *Sustainable Chemistry and Pharmacy*, 16, 100261. DOI: 10.1016/j.scp.2020.100261.

[10] Liu, Y., Zhao, X., Li, J., Ma, D., Han, R. (2012). Characterization of bio-char from pyrolysis of wheat straw and its evaluation on methylene blue adsorption. *Desalination and Water Treatment*, 46 (1-3), 115–123. DOI: 10.1080/19443994.2012.677408.

[11] Taghizadeh, F. (2016). The Study of Structural and Magnetic Properties of NiO Nanoparticles. *Optics and Photonics Journal*, 6(8), 164–169. DOI: 10.4236/opj.2016.68b027.

[12] Sahoo, Y. (2015). An aerosol-mediated magnetic colloid: Study of nickel nanoparticles. *Journal of Applied Physics*, 98(5), 054308. DOI: 10.1063/1.2033145.

[13] Wang, H., Kou, X., Zhang, J., Li, J. (2008). Large scale synthesis and characterization of Ni nanoparticles by solution reduction method. *Bulletin of Materials Science*, 31(1) 97–100. DOI: 10.1007/s12034-008-0017-1.

[14] Som, A.M., Wang, Z., Al-Tabbaa, A. (2013). Palm frond biochar production and characterization. *Earth and Environmental Science Transactions of The Royal Society of Edinburgh*, 103(1), 39–48. DOI: 10.1017/S1755691012000035.

[15] Sewu, D.D., Boakye, P., Woo, S.H. (2017). Highly efficient adsorption of cationic dye by biochar produced with Korean cabbage waste. *Bioresource Technology*, 224, 206–213. DOI: 10.1016/j.biortech.2016.11.009.

[16] Fidel, R.B., Laird, D.A., Thompson, M.L. (2013). Evaluation of modified boehm titration methods for use with biochars. *Journal of Environmental Quality*, 42(6), 1771–1778. DOI: 10.2134/jeq2013.07.0285.

[17] Mian, M.M., Liu, G. (2018). Recent progress in biochar-supported photocatalysts: Synthesis, role of biochar, and applications. *RSC Advances*, 8 (26), 14237–14248. DOI: 10.1039/c8ra02258e.

[18] Murnieks, R., Apseniece, L., Kampars, V., Shustere, Z., Malins, K. (2016). Investigation of Deoxygenation of Rapeseed Oil over Raney Nickel and Ni/SiO_2–Al_2O_3 Catalysts. *Arabian Journal for Science and Engineering*, 41(6), 2193–2198. DOI: 10.1007/s13369-015-1932-2.

[19] Likasari, I.D., Astuti, R.W., Yahya, A., Isnaini, N., Purwiandono, G., Hidayat, H., Wicaksono, W.P., Fatimah, I. (2021). NiO nanoparticles synthesized by using Tagetes erecta L leaf extract and their activities for photocatalysis, electrochemical sensing, and antibacterial features. *Chemical Physics Letters*, 780, 138914. DOI: 10.1016/j.cplett.2021.138914.

[20] Zhang, L., Ren, Y., Xuen, Y., Cui, Z., Hui, Q., Han, C., He, J. (2020). Preparation of biochar by mango peel and its adsorption characteristic of Cd(II) in solution. *RSC Advances*, 10, 35878. DOI: 10.1039/D0RA06586B.

[21] Zhong, Z., Yu, G., Mo, W., Zhang, C., Huang, H., Li, S., Lu, X., Zhang, P., ZHu, H. (2019). Enhanced phospate sequestration by Fe(III) modified biochar derived from coconut shell. *RSC Advances*, 9, 10425. DOI: 10.1039/C8RA10400J.

[22] Wang, Z., Yang, X., Qin, T., Liang, G., Li, Y., Xie, X. (2019). Efficient removal of oxytetracycline from aqueous solution by a novel magnetic clay–biochar composite using natural attapulgite and cauliflower leaves. *Environmental Science and Pollution Research*, 26(8), 7463–7475. DOI: 10.1007/s11356-019-04172-8.

[23] Premarathna, K.S.D., Rajapaksha, A.U., Sakar, B., Kwon, E.E., Bhatnagar, A., Ok, Y.S., Vintanage, S. (2019). Biochar-Based Engineered Composites for Sorptive Decontamination of Water: A Review. *Chemical Engineering Journal*, 372, 536–550. DOI: 10.1016/j.cej.2019.04.097.

[24] Chen, M., Tao, X., Wang, D., Xu, Z., Xu, X., Hua, X., Xu, H,C., Xi, N., Cao, X. (2019). Facilitated transport of cadmium by biochar-Fe3O4 nanocomposites in water-saturated natural soils. *Science of The Total Environment*, 684, 265–275. DOI: 10.1016/j.scitotenv.2019.05.326.

[25] Wang, W., Liu, Y. , Wang, Y., Liu, L., Hu, C. (2021). Effect of nickel salts on the production of biochar derived from alkali lignin: properties and applications. *Bioresource Technology*, 341, 125876. DOI: 10.1016/j.biortech.2021.125876.

[26] Liu, J., He, Y., Ma, X., Liu, G., Yao, Y., Liu, H., Chen, H., Huang, Y., Chen, C., Wang, W. (2016). Catalytic pyrolysis of tar model compound with various bio-char catalysts to recycle char from biomass pyrolysis. *BioResources*, 11(2), 3752–3768. DOI: 10.15376/biores.11.2.3752-3768.

[27] Behazin, E., Ogunsona, E., Rodriguez-Uribe, A., Mohanty, A.K., Misra, M., Anyia, A.O. (2016). Mechanical, chemical, and physical properties of wood and perennial grass biochars for possible composite application. *BioResources*, 11(1), 1334–1348. DOI: 10.15376/biores.11.1.1334-1348.

[28] Chang, C.C., Cho, H.J., Wang, Z., Wang, X., Fan, W. (2015). Fluoride-free synthesis of a Sn-BEA catalyst by dry gel conversion. *Green Chemistry*, 17(5), 2943–2951. DOI: 10.1039/c4gc02457e.

[29] Zhang, H., Lin, H., Zheng, Y. (2014). The role of cobalt and nickel in deoxygenation of vegetable oils. *Applied Catalysis B: Environmental*, 160–161, 415–422. DOI: 10.1016/j.apcatb.2014.05.043.

[30] Kamaruzaman, M.F., Taufiq-Yap, Y.H., Derawi, D. (2019). Green diesel production from palm fatty acid distillate over SBA-15-supported nickel, cobalt, and nickel/cobalt catalysts. *Biomass and Bioenergy*, 134, 105476. DOI:10.1016/j.biombioe.2020.105476.

[31] Itthibenchapong, V., Srifa, A., Kaewmeesri, R., Kidkhunthod, P., Faungnawakij, K. (2016). Deoxygenation of palm kernel oil to jet fuel-like hydrocarbons using Ni-MoS_2/γ-Al_2O_3 catalysts. *Energy Conversion and Management*, 134, 188–196. DOI: 10.1016/j.enconman.2016.12.034.

[32] Aiamsiri, P., Tumnantong, D., Yoosuk, B., Ngamcharussrivichai, C., Prasassarakich, P. (2021). Biohydrogenated Diesel from Palm Oil Deoxygenation over Unsupported and γ-Al_2O_3 Supported Ni–Mo Catalysts. *Energy & Fuels*, 35(18), 14793–14804. DOI: 10.1021/acs.energyfuels.1c02083.

[33] Asikin-Mijan, N., Lee, H.V., Abdulkareem-Alsultan, G., Afandi, A., Taufiq-Yap, Y.H. (2017). Production of green diesel via cleaner catalytic deoxygenation of Jatropha curcas oil. *Journal of Cleaner Production*, 167, 1048–1059. DOI: 10.1016/j.jclepro.2016.10.023.

[34] Nugrahaningtyas, K.D., Lukitawati, R., Mukhsin, S.A., Fadlulloh, Z., Sabiilagusti, A.I., Budiman, A.W., Kurniawai, M.F. (2022). Conversion of waste cooking oil into green diesel using Ni/MOR and Cu/MOR catalysts. *Journal of Physics: Conference Series*, 2190(1), 012037. DOI: 10.1088/1742-6596/2190/1/012037.

[35] Wang, M., He, M., Fang, Y., Baeyens, J., Tan, T. (2017). The Ni-Mo/γ-Al_2O_3 catalyzed hydrodeoxygenation of FAME to aviation fuel. *Catalysis Communications*, 100, 237–241. DOI: 10.1016/j.catcom.2017.07.009.